PERGAMON

International Journal of Solids and Structures 38 (2001) 5469–5480

INTERNATIONAL JOURNAL OF SOLIDS and STRUCTURES

www.elsevier.com/locate/ijsolstr

Form finding of membrane structures by the updated reference method with minimum mesh distortion

J. Bonet [a,*], J. Mahaney [b]

[a] *Department of Civil Engineering, University of Wales, Singleton Park, Swansea SA2 8PP, UK*
[b] *Mercer University, Macon, Georgia, USA*

Received 14 August 2000; in revised form 16 October 2000

Abstract

This paper presents a new technique for the solution of the well-known form finding problem in membrane structures. The technique proposed is based on the updated reference configuration method proposed by Bletzinger [Proceedings of the IASS Colloquium on Structural Morphology: Towards the New Millenium, Nottingham, 1997] in which an area functional is minimised within the context of a finite element discretisation. In this paper an additional functional term is introduced with the aim of minimising the mesh distortion during the form finding process. This new term provides in-plane stiffness which prevents the emergence of mechanisms without the need for ad hoc changes of the tangent matrix. As a consequence of this additional strain energy term, the form finding process can be viewed as a standard large strain membrane analysis with a specific choice of hyperelastic strain energy function. This implies that it can be implemented in any standard code as an additional constitutive model. Two well-known simple examples of form finding will be presented to illustrate the method proposed.

Keywords: Form finding; Membranes; Tension structures; Large strain; Hyperelasticity

1. Introduction

Form finding is a well-known mathematical problem (see for instance Otto, 1967). It implies finding the surface with a minimum area for a given fixed boundary. In physical terms it results in surfaces which, like soap films, are in self-equilibrium with a uniform state of isotropic stress. The problem is of engineering significance in the design of tension membrane structures, which are becoming increasingly popular as an attractive way of providing temporary or semi-permanent cover for outdoor areas.

Traditionally, form finding has been solved using dynamic relaxation techniques in the context of simple truss networks or linear triangular meshes (Barnes, 1975; Wakefield, 1979, 1998). The above techniques require specialist software and have no reliable means of controlling the in-plane distortion of the finite element mesh used to describe the membrane. More recently Tabarrok and Qin (1992) and Bletzinger

* Corresponding author. Fax: +44-1792-295-676.
E-mail addresses: j.bonet@swansea.ac.uk (J. Bonet), mahaney_jm@mercer.edu (J. Mahaney).

0020-7683/01/$ - see front matter
PII: S0020-7683(00)00382-6

(1997) have proposed techniques based on an incremental Newton–Raphson method. In particular Bletzinger (1997) has introduced the concept of updated reference configuration as an artificial initial membrane position, which is iteratively updated during the form finding process. An extensive set of references on the subject of form finding can be found in Motro (1999).

The problem of in-plane mesh distortion can be easily illustrated by considering the case where the prescribed boundary happens to lie on a plane. Obviously, the solution is then a flat surface on the same plane. Unfortunately, the nodes of a finite element description of this surface can lie anywhere on this plane without affecting the solution. This implies a lack of in-plane stiffness of the finite element model leading to a singular tangent stiffness matrix. In Bletzinger (1997) this problem is overcome by a modification of the initial stress component of the tangent stiffness based on the artificial reference configuration.

The technique proposed in this paper is similar to the method introduced by Bletzinger in that a functional describing the total mesh area is constructed and minimised with a standard Newton–Raphson process. However, in-plane stiffness is provided by an additional functional which measures the amount of shear distortion in the model from the initial or reference configuration to the current shape. In this way, minimising the combined functional leads to a balance between minimum area and minimum shear distortion in the mesh. At the end of the analysis the final surface shape can be used as a new reference configuration and the solution process is in this way iteratively repeated until the area is minimised. The method proposed can be viewed as a specific case of a hyperelastic constitutive equation for membranes and can therefore be easily implemented within the context of standard finite element large strain membrane analysis (see for instance Oden and Sato, 1967; Argyris et al., 1977; Gruttman and Taylor, 1992; De Souza Neto et al., 1995; Kyriacou et al., 1996; Bonet et al., 2000).

In order to illustrate the technique proposed, two well-known examples will be described: a catenoid (or revolution catenary) and Scherk's surface (see for instance Bletzinger, 1997). In the first case a comparison against the analytical solution will be shown and in both cases the convergence of the area and distortion energy will be plotted as the form finding process takes place.

2. Area minimisation

The aim of this section is to define the main functional which, after minimisation, will lead to a minimum surface area. The section will show how this functional can be expressed in the form of a pseudo-hyperelastic constitutive equation for which the corresponding Cauchy stresses are uniform and isotropic, that is, no shear stress is present in the membrane.

2.1. Area functional

Consider a general membrane in its current configuration as shown in Fig. 1. The geometry of the membrane is defined by a mapping $\boldsymbol{x} = \phi(\boldsymbol{\xi})$ from a two-dimensional parametric plane to its current configuration. In order to minimise the total surface area, the following functional Π_a is defined:

$$\Pi_a(\phi) = N_0 \int_a \mathrm{d}a \tag{1}$$

where N_0 represents an arbitrary parameter chosen to have units of force per unit length so that it will later describe the value of the final uniform stresses on the membrane at the equilibrium configuration. (Note that the term stress will be used throughout to denote force per unit membrane length. In this way any reference to the membrane thickness, which is irrelevant to form finding problems, will be avoided.)

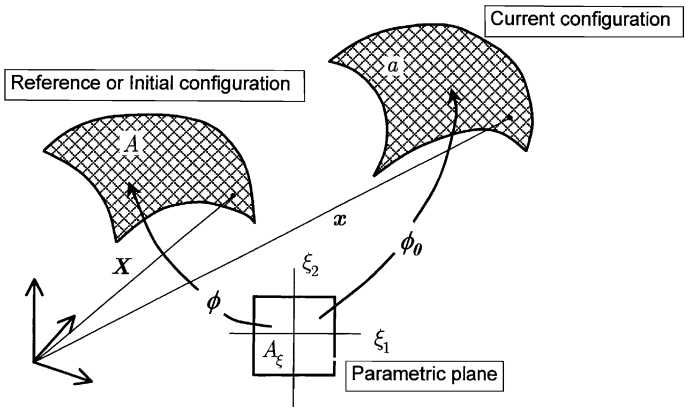

Fig. 1. Membrane geometry definition.

The current element of area can be related to the area in the parametric plane by means of the determinant of the metric tensor $\boldsymbol{C}$ (also known as the Cauchy–Green deformation tensor, see for instance Bonet and Wood, 1997) as:

$$\mathrm{d}a = \sqrt{\det \boldsymbol{C}}\,\mathrm{d}A_\xi \tag{2}$$

where $\boldsymbol{C}$ is defined as:

$$\boldsymbol{C} = \boldsymbol{F}^{\mathrm{T}}\boldsymbol{F}; \qquad \boldsymbol{F} = \nabla_\xi \phi = \frac{\partial \phi}{\partial \boldsymbol{\xi}} \tag{3}$$

Eq. (2) enables the functional defined by Eq. (1) to be rewritten as:

$$\Pi_a(\phi) = N_0 \int_a \sqrt{\det \boldsymbol{C}}\,\mathrm{d}A_\xi \tag{4}$$

With the eventual aim of constructing an artificial constitutive model that recreates the area functional defined by Eq. (1), consider an arbitrary reference membrane configuration as shown in Fig. 1. This configuration can be interpreted as the starting position of the membrane in a fictitious large strain deformation process and is defined by a mapping $\boldsymbol{X} = \phi_0(\boldsymbol{\xi})$ with associated Cauchy–Green deformation tensor $\boldsymbol{C}_0$ given by:

$$\boldsymbol{C}_0 = \boldsymbol{F}_0^{\mathrm{T}}\boldsymbol{F}_0; \qquad \boldsymbol{F}_0 = \nabla_\xi \phi_0 = \frac{\partial \phi_0}{\partial \boldsymbol{\xi}} \tag{5}$$

The element of area at this artificial reference configuration is related to the element of area at the parametric plane via the equation:

$$\mathrm{d}A = \sqrt{\det \boldsymbol{C}_0}\,\mathrm{d}A_\xi \tag{6}$$

This enables the area functional (4) to be expressed in the form of a strain energy potential from the artificial initial configuration to the final membrane state as:

$$\Pi_a(\phi) = \int_A \Psi_a(\boldsymbol{C}, \boldsymbol{C}_0)\,\mathrm{d}A \tag{7}$$

where the pseudo-strain energy function per unit initial volume is easily derived by combining Eqs. (4) and (6) to give, after simple algebra:

$$\Psi_a(\boldsymbol{C}, \boldsymbol{C}_0) = N_0 \sqrt{\det(\boldsymbol{C}\boldsymbol{C}_0^{-1})} \tag{8}$$

Note that despite the appearance of $\boldsymbol{C}_0$ in the definition of this strain energy function, the actual final functional $\Pi_a(\phi)$ is in fact entirely independent of the initial configuration chosen.

2.2. Stress tensor

The minimisation of functional (7) with respect to the final membrane configuration is expressed in terms of the directional derivative of Π_a in the direction of an arbitrary virtual velocity $\delta\boldsymbol{v}$ compatible with the boundary conditions as:

$$D\Pi_a[\delta\boldsymbol{v}] = \frac{\mathrm{d}}{\mathrm{d}\varepsilon}\bigg|_{\varepsilon=0} \Pi_a(\phi + \varepsilon\delta\boldsymbol{v}) = 0 \tag{9}$$

Substituting the area functional into the above equation from Eq. (7) yields, after simple algebraic manipulations, the equilibrium equation as:

$$D\Pi_a[\delta\boldsymbol{v}] = \int_A \boldsymbol{F}\boldsymbol{S}_a(\boldsymbol{C}, \boldsymbol{C}_0) : \nabla_\xi \delta\boldsymbol{v}\, \mathrm{d}A = 0 \tag{10}$$

where the term $\boldsymbol{S}_a$ denotes the second Piola–Kirchhoff stress at the parametric plane and is defined as:

$$\boldsymbol{S}_a = 2\frac{\partial \Psi_a(\boldsymbol{C}, \boldsymbol{C}_0)}{\partial \boldsymbol{C}} = 2N_0 \frac{\partial}{\partial \boldsymbol{C}} \left[\sqrt{\det(\boldsymbol{C}\boldsymbol{C}_0^{-1})} \right] \tag{11}$$

After tedious but standard algebra (see for instance Bonet et al., 2000), the second Piola–Kirchhoff tensor emerges from the above equation to give:

$$\boldsymbol{S}_a = N_0 \sqrt{\det(\boldsymbol{C}\boldsymbol{C}_0^{-1})}\, \boldsymbol{C}^{-1} \tag{12}$$

Although Eqs. (10) and (12) can be used as the basis for a finite element discretisation, it is instructive to rewrite the equilibrium Eq. (10) with respect to the current configuration. For this purpose, note first that the gradient of the virtual velocity with respect to the parametric coordinates can be related to the standard Cartesian gradient as:

$$\nabla_\xi \delta\boldsymbol{v} = (\nabla \delta\boldsymbol{v})\boldsymbol{F} \tag{13}$$

With the help of this equation it is easy to show that the equilibrium equation can be equally expressed in the final membrane configuration in terms of the Cauchy stress tensor $\boldsymbol{\sigma}_a$ as:

$$D\Pi_a[\delta\boldsymbol{v}] = \int_a \boldsymbol{\sigma}_a : \nabla \delta\boldsymbol{v}\, \mathrm{d}a = 0; \qquad \boldsymbol{\sigma}_a = \left(\frac{\mathrm{d}A}{\mathrm{d}a}\right) \boldsymbol{F}\boldsymbol{S}_a\boldsymbol{F}^{\mathrm{T}} \tag{14}$$

Substituting Eq. (12) into the second part of the above equation and using Eqs. (2) and (6) for the initial and current area, as well as Eq. (3) for the current Cauchy–Green tensor gives the Cauchy stress tensor as:

$$\boldsymbol{\sigma}_a = N_0 \boldsymbol{I} \tag{15}$$

where $\boldsymbol{I}$ denotes the unit or identity matrix. It is clear from the above equation that, as intended, the state of stresses that results from the pseudo-strain energy functional defined above is uniform and isotropic throughout the membrane.

2.3. Constitutive tensor

Eq. (10) is clearly nonlinear with respect to the current membrane configuration. Its solution in the context of a finite element procedure will therefore be based on a Newton–Raphson type of iteration. This iterative process will necessitate the second derivative of the functional in order to construct a suitable tangent stiffness matrix. For this purpose, Eq. (10) is differentiated in the direction of an arbitrary incremental displacement $\boldsymbol{u}$ from the current configuration to give,

$$D^2\Pi_a[\delta\boldsymbol{v},\boldsymbol{u}] = \int_A (\boldsymbol{F}^{\mathrm{T}}\nabla_\xi \boldsymbol{u}) : \mathbb{C}_a : (\boldsymbol{F}^{\mathrm{T}}\nabla_\xi \delta v)\,\mathrm{d}A + \int_A \boldsymbol{S}_a : \left[(\nabla_\xi \boldsymbol{u})^{\mathrm{T}}(\nabla_\xi \delta\boldsymbol{v})\right]\mathrm{d}A \tag{16}$$

The second term in the equation above will lead to the initial stress matrix after suitable finite element discretisation, whereas the first term contains the Lagrangian elasticity tensor $\mathbb{C}_a$ defined by:

$$\mathbb{C}_a = 2\frac{\partial \boldsymbol{S}_a}{\partial \boldsymbol{C}} = 2N_0\frac{\partial}{\partial \boldsymbol{C}}\left[\sqrt{\det(\boldsymbol{C}\boldsymbol{C}_0^{-1})}\,\boldsymbol{C}^{-1}\right] = N_0\sqrt{\det(\boldsymbol{C}\boldsymbol{C}_0^{-1})}\left[\boldsymbol{C}^{-1}\otimes\boldsymbol{C}^{-1} - \mathscr{G}\right] \tag{17}$$

and the fourth order tensor $\mathscr{G}$ is:

$$\mathscr{G} = -2\frac{\partial \boldsymbol{C}^{-1}}{\partial \boldsymbol{C}}; \qquad \mathscr{G}_{IJKL} = (\boldsymbol{C}^{-1})_{IK}(\boldsymbol{C}^{-1})_{JL} + (\boldsymbol{C}^{-1})_{IL}(\boldsymbol{C}^{-1})_{JK} \tag{18}$$

3. Distortion minimisation

The functional defined above should in theory lead to a membrane configuration that minimises the total surface area. However, in practice a solution can rarely be achieved as the tangent operator defined in Section 2 is in fact singular. This singularity is easily illustrated in the trivial case where the boundary conditions are such that the analytical solution is a plane. In this case, any movement or displacement of the membrane on the plane and within the designated fixed boundary will lead to the same total surface area. Physically, all such movements are energy free and, consequently, the deformation model described so far contains an infinite number of in plane mechanisms. In practical terms, the stiffness matrix that will emerge from the finite element discretisation of Eq. (16) will be singular. This singularity has been circumvented in Bletzinger (1997) by artificially modifying the initial stress component of the tangent stiffness matrix. Although this procedure removes the singularity of the tangent matrix and appears to work satisfactorily in many cases, no additional terms are added to the internal forces used to obtain equilibrium. Hence, the inherent lack of in-plane stiffness is still present in the equations.

The procedure developed here is more robust and is based on the definition of an additional distortion energy that will provide the required in-plane stiffness. This new strain energy term is defined in such a way that it leads to purely deviatoric stresses. In this way it will interfere as little as possible with the isotropic stress N_0 defined above which is the one responsible for driving the membrane towards an equilibrium position that minimises the total surface area.

3.1. Distortion

Consider again the fictitious deformation of the membrane from the arbitrary initial configuration to the final position. In order to define the distortion strain energy, it is first necessary to isolate the area preserving component of this deformation process. Following the standard procedure described in detail in Bonet and Wood (1997), the isochoric component of the right Cauchy–Green tensor is defined as:

$$\hat{\boldsymbol{C}} = (\det \boldsymbol{C})^{-1/2}\,\boldsymbol{C}; \qquad \hat{\boldsymbol{C}}_0 = (\det \boldsymbol{C}_0)^{-1/2}\,\boldsymbol{C}_0 \tag{19}$$

Note that by construction $\det \boldsymbol{C} = \det \boldsymbol{C}_0 = 1$.

3.2. Distortion functional

In order to correct the rank deficiency of the surface area functional, an augmented functional is now defined as:

$$\Pi(\phi, \phi_0) = \Pi_a(\phi) + \Pi_{\text{dis}}(\phi, \phi_0); \qquad \Pi_{\text{dis}}(\phi, \phi_0) = \int_A \Psi_{\text{dis}}(\hat{\boldsymbol{C}}, \hat{\boldsymbol{C}}_0)\,\mathrm{d}A \tag{20}$$

where the distortion strain energy Ψ_{dis} can, for instance, be defined using the neo-Hookean model commonly used to describe hyperelastic rubber (Bonet et al., 2000) to give,

$$\Psi_{\text{dis}}(\hat{\boldsymbol{C}}, \hat{\boldsymbol{C}}_0) = \frac{1}{2}\mu(\hat{\boldsymbol{C}} : \hat{\boldsymbol{C}}_0^{-1} - 2) \tag{21}$$

The coefficient μ in this expression describes a fictitious shear modulus of the membrane. Clearly, the ratio between μ and N_0 determines the relative importance of each term in Eq. (20). The smaller this ratio is, the less effect the above distortion functional will have over the final equilibrium configuration. Ideally, one should take $\mu = 0$ in order to ensure that the equilibrium position coincides with the minimum surface. As this is not possible, one should use as small a value as possible compatible with a nonsingular tangent modulus. Practical advice on how to achieve this will be given in the following sections.

It is also crucial to note that, unlike the area functional defined in Section 2, the distortion functional is not independent of the chosen reference configuration. In fact, the value of the distortion strain energy returned by Eq. (21) will be small if the reference configuration is chosen to be close to the final equilibrium configuration. This fact will be used in Section 4 to define an iterative scheme whereby the reference configuration is continuously updated. This iterative procedure will ensure the final solution is independent of the artificial shear modulus chosen.

3.3. Deviatoric stress tensor

The minimisation of the augmented functional now leads to an equilibrium equation similar in form to expression (10) but with an additional deviatoric second Piola–Kirchhoff stress tensor term as:

$$D\Pi[\delta \boldsymbol{v}] = \int_A \boldsymbol{F}\boldsymbol{S} : \nabla_\xi \delta \boldsymbol{v}\,\mathrm{d}A = 0; \quad \boldsymbol{S} = \boldsymbol{S}_a + \boldsymbol{S}' \tag{22}$$

where $\boldsymbol{S}'$ emerges from the differentiation of the distortion strain energy with respect to the right Cauchy–Green tensor to give,

$$\boldsymbol{S}' = 2\frac{\partial \Psi_{\text{dis}}(\boldsymbol{C}, \boldsymbol{C}_0)}{\partial \boldsymbol{C}} = \mu \frac{\partial}{\partial \boldsymbol{C}}\left[\frac{\sqrt{\det \boldsymbol{C}_0}}{\sqrt{\det \boldsymbol{C}}}(\boldsymbol{C} : \boldsymbol{C}_0^{-1})\right] \tag{23}$$

which after simple algebra leads to,

$$\boldsymbol{S}' = \mu \frac{\sqrt{\det \boldsymbol{C}_0}}{\sqrt{\det \boldsymbol{C}}}[\boldsymbol{C}_0^{-1} - \tfrac{1}{2}(\boldsymbol{C} : \boldsymbol{C}_0^{-1})\boldsymbol{C}^{-1}] \tag{24}$$

Note that this tensor is only deviatoric with respect to the metric $\boldsymbol{C}$, that is $\boldsymbol{S}' : \boldsymbol{C} = 0$, but its trace is in general different from zero. The corresponding deviatoric Cauchy stress tensor is obtained using the second part of Eq. (14) to give:

$$\boldsymbol{\sigma}' = \mu \frac{\det \boldsymbol{C}_0}{\det \boldsymbol{C}} [\boldsymbol{F}\boldsymbol{C}_0^{-1}\boldsymbol{F}^{\mathrm{T}} - \tfrac{1}{2}(\boldsymbol{C} : \boldsymbol{C}_0^{-1})\boldsymbol{I}] \tag{25}$$

It is a simple exercise to show that the trace of $\boldsymbol{\sigma}'$ as defined above is indeed zero. Note also that as the reference configuration approaches the final configuration $\boldsymbol{C}_0$ will tend to $\boldsymbol{C}$ and therefore $\boldsymbol{\sigma}'$ will approach zero.

3.4. Deviatoric constitutive tensor

Finally, it is necessary to obtain the second derivative of the augmented functional in order to develop a Newton–Raphson type of nonlinear iteration. For this purpose, differentiation of Eq. (22) now leads to:

$$D^2\Pi[\delta\boldsymbol{v}, \boldsymbol{u}] = \int_A (\boldsymbol{F}^{\mathrm{T}}\nabla_\xi \boldsymbol{u}) : \mathbb{C} : (\boldsymbol{F}^{\mathrm{T}}\nabla_\xi \delta\boldsymbol{v})\, \mathrm{d}A + \int_A \boldsymbol{S} : \left[(\nabla_\xi \boldsymbol{u})^{\mathrm{T}}(\nabla_\xi \delta\boldsymbol{v})\right] \mathrm{d}A \tag{26}$$

where the total elasticity tensor $\mathbb{C}$ is made up of the area component defined in Section 2.3 plus the distortion component given by:

$$\mathbb{C} = \mathbb{C}_a + \mathbb{C}_{\mathrm{dis}}; \quad \mathbb{C}_{\mathrm{dis}} = 2\frac{\partial \boldsymbol{S}'}{\partial \boldsymbol{C}} \tag{27}$$

Differentiation of Eq. (24) leads eventually to the distortion elasticity tensor for the neo-Hokean model as:

$$\mathbb{C}_{\mathrm{dis}} = \mu \frac{\sqrt{\det \boldsymbol{C}_0}}{\sqrt{\det \boldsymbol{C}}} [\tfrac{1}{2}(\boldsymbol{C} : \boldsymbol{C}_0^{-1})(\boldsymbol{C}^{-1} \otimes \boldsymbol{C}^{-1} + \mathscr{G}) - \boldsymbol{C}_0^{-1} \otimes \boldsymbol{C}^{-1} - \boldsymbol{C}^{-1} \otimes \boldsymbol{C}_0^{-1}] \tag{28}$$

4. Solution process

4.1. Newton–Raphson iteration

The minimisation of the combined area and shear distortion functional defined in Eq. (20) is achieved within the context of a standard large strain finite element formulation (see for instance, Bonet et al., 2000). Consequently, all kinematic variables, current and initial geometries, virtual velocities and displacements are interpolated from nodal values via standard shape functions $N_I(\xi_1, \xi_2)$; $I = 1, \ldots, n$. In this way the equilibrium or first variation Eq. (22) becomes, after discretisation,

$$\boldsymbol{T}_I(\boldsymbol{x}_J) = \int_A \boldsymbol{F}\boldsymbol{S}\nabla_\xi \boldsymbol{N}_I \, \mathrm{d}A = 0 \tag{29}$$

And a Newton–Raphson solution process is described by the standard update equations:

$$\sum_{J=1}^{N} \boldsymbol{K}_{IJ}\boldsymbol{u}_J = -\boldsymbol{T}_I\left(\boldsymbol{x}_K^{(k)}\right); \qquad \boldsymbol{x}_I^{(k+1)} = \boldsymbol{x}_I^{(k)} + \boldsymbol{u}_I \tag{30}$$

where the tangent stiffness matrix is obtained from the discretisation of Eq. (26) as:

$$K_{IJ}^{ij} = \sum_{\alpha,\beta,\gamma,\delta=1}^{2} \left(\int_A \frac{\partial x_i}{\partial \xi_\beta} \frac{\partial N_I}{\partial \xi_\alpha} \mathbb{C}_{\alpha\beta\gamma\delta} \frac{\partial x_j}{\partial \xi_\delta} \frac{\partial N_J}{\partial \xi_\beta} \, \mathrm{d}A \right) + \delta_{ij} \int_A \nabla_\xi N_I \cdot (\boldsymbol{S}\nabla_\xi N_J) \, \mathrm{d}A \tag{31}$$

4.2. Form finding algorithm

In a typical form finding process, it is usually convenient, but not necessary, to start from a flat initial mesh, as this can be more easily generated. The boundary constraints are then enforced as imposed displacements on the boundary mesh points. If necessary, this can be achieved in a number of 'load' steps to facilitate the convergence of the Newton–Raphson iteration. This initial 'set-up' phase is no different from any standard large strain membrane analysis, with the exception that a very specific constitutive model is used.

Once the boundary has reached its required position, a number of form finding steps are then necessary to reach the final minimum surface. In each step the reference configuration is chosen as the final shape on the previous step. In this way, the distortion component of the energy functional refers only to the incremental motion of the surface and, as the shape converges to the final minimum surface, will have a decreasing influence on the process. In the final steps, the incremental movement is minimal and it is essentially the area functional (which is independent of the reference configuration) that is being minimised. Note however, that even when the distortional contribution to the equilibrium equations is very small, its contribution to the in-plane terms of the stiffness matrix does not diminish. This ensures that the tangent matrix is not singular during the process.

5. Examples

5.1. Catenoid

The catenoid, or catenary of revolution, is a classic form finding problem, discussed in many authors, such as Otto (1967) and Bletzinger (1997). Fig. 2 shows the catenoid with an inner radius of 5, an outer radius of 15, and a height of 8. The mesh, initially planar, is unstructured, using 341 nodes and 613 linear triangular elements. Given the axial symmetry of the problem only a quarter of the model is solved. Both μ and N_0 are set equal to 1.0.

The initial set-up takes place over 10 steps, during which the inner radius is raised from a height of 0 to the maximum height of 8. Form finding takes places over eight more steps. A cut through the final shape is compared against the analytical solution in Fig. 3, which shows an excellent agreement. Note that the mesh is well distributed and all the elements have a 'reasonable' shape. For comparison the profile obtained with a courser mesh containing only 103 elements is also shown. Fig. 4 shows the logarithmic decrease in shear and area energy during form finding. Note that as predicted the shear or distortional energy becomes

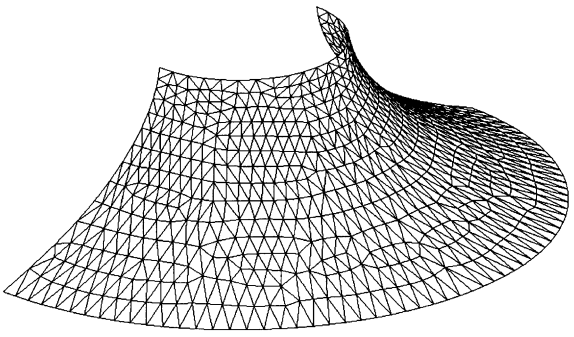

Fig. 2. Catenoid.

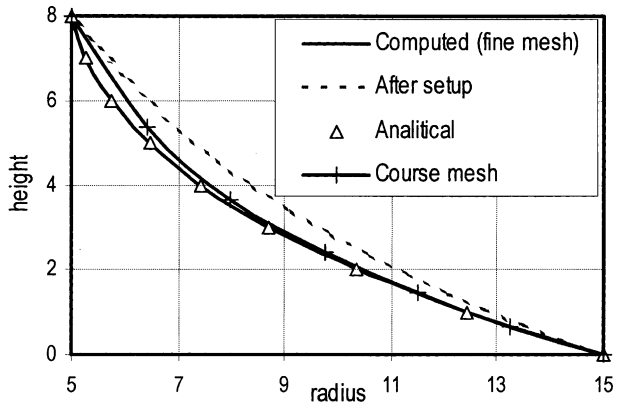

Fig. 3. Catenoid – analytical comparison.

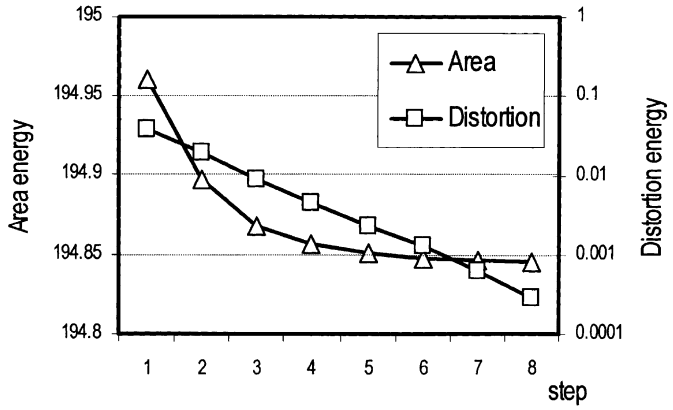

Fig. 4. Catenoid – energy minimisation.

smaller as more form finding steps are taken. The final area achieved was 194.845, which is within 0.005% of the exact area of 194.8547.

5.2. Scherk's surface

Like the catenoid, Scherk's surface is a classic form finding problem (Lewis, 1997; Bletzinger, 1997; Maurin and Motro, 1997). In the example chosen here, the boundary is described by a unit cube. Again, for convenience, the process starts from flat meshes in which boundary nodes are incrementally moved to their final positions. Two meshes have been used in this example: a triangular mesh with 1200 elements and a quadrilateral mesh consisting of 662 bilinear quads. The resulting final configurations are shown in Figs. 5 and 6. In both cases $N_0 = \mu = 1$.

The convergence rates of the area and distortional energies are shown in Figs. 7 and 8 respectively for both meshes. The final areas of the quad and triangular meshes were 2.47101 and 2.47039 respectively.

In order to illustrate the importance of the shear distortional energy, the form finding process for the quad mesh is repeated but now the value of μ is linearly decreased every step down to 0.0025 in the final step. The resulting shape is shown in Fig. 9 and clearly displays excessive mesh distortion. It is interesting to

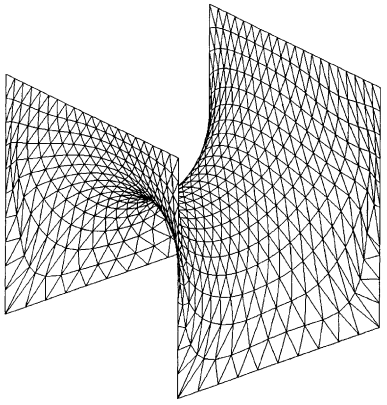

Fig. 5. Scherk's surface – triangular mesh.

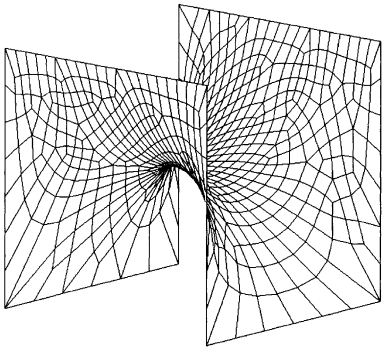

Fig. 6. Scherk's surface – quadrilaterals.

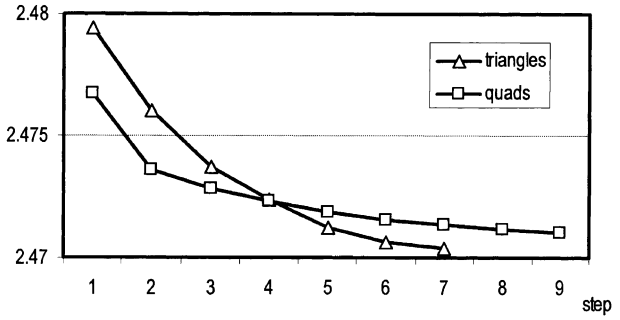

Fig. 7. Scherk's surface – area energies.

observe that a similar detrimental effect to lowering the value of μ is not observed for the case of triangular meshes. In the case shown in Fig. 5, the value of μ can be lowered during the form finding steps without the appearance of significant mesh distortions.

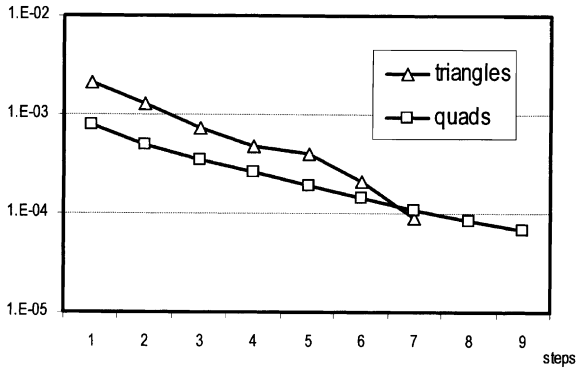

Fig. 8. Scherk's surface – distortion energies.

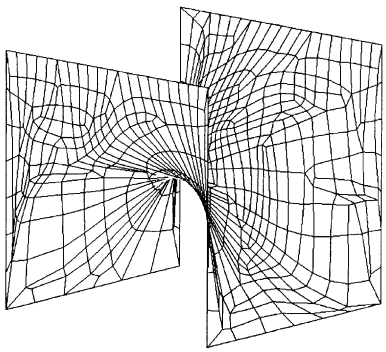

Fig. 9. Scherk's surface – low shear modulus.

6. Concluding remarks

The paper has presented a new technique for the solution of the form finding problem expressed as a surface with minimum area. The methods proposed leads to the definition of an artificial large strain hyperelastic constitutive model with two components, namely area strain energy and shear strain energy. The first term simply measures the surface area whereas the second component gives a measure of the incremental distortion from an arbitrary reference configuration. This second term is responsible for introducing in-plane stiffness to the problem and preventing the tangent matrix from becoming singular. As the reference configuration is iteratively updated in a sequence of form finding steps, the shear component of the functional becomes less significant but still provides the necessary stiffness.

The algorithm has been demonstrated with the help of two well-known geometrical problems, namely a Catenoid and Scherk's surface. Solutions using triangular and quadrilateral meshes have been obtained and compared. For the Catenoid an analytical comparison is provided to demonstrate that the method proposed converges to the analytical solution.

Acknowledgements

The authors would like to express their gratitude to Dr. R.D. Wood for many useful discussions.

References

Argyris, J.H., Dunne, P.C., Maasse, M., Orkisz, J., 1977. Higher order simplex elements for large strain – natural approach. Comp. Meth. Appl. Mech. Engng. 16, 369–403.

Barnes, M.R., 1975. Applications of dynamic relaxation to the design and analysis of cable, membrane and pneumatic structures. Proc. Int. Conf. Space Struct., Guildford.

Bletzinger, K.-U., 1997. Form finding of membrane structures and minimal surfaces by numerical continuation. Proc. IASS Coll. Structural Morphology: Towards the New Millennium, Nottingham.

Bonet, J., Wood, R.D., 1997. Nonlinear Continuum Mechanics for Finite Element Analysis. Cambridge University Press, Cambridge.

Bonet, J., Wood, R.D., Mahaney, J., Heywood, P., 2000. Finite element analysis of air supported membrane structures. Comp. Meth. Appl. Mech. Engng. 47, 1–17.

De Souza Neto, E.A., Peric, D., Owen, D.R.J., 1995. Finite elasticity in spatial description: linearization aspects with 3-D membrane applications. Int. J. Num. Meth. Engng. 38, 3365–3381.

Gruttmann, F., Taylor, R.L., 1992. Theory and finite element formulation of rubberlike membrane shells using principal stretches. Int. J. Num. Meth. Engng. 35, 1111–1126.

Kyriacou, S.K., Schwab, C., Humphrey, J.D., 1996. Finite element analysis of nonlinear orthotropic hyperelastic membranes. Computat. Mech. 18 (4), 269–278.

Lewis, W.J., Lewis, T.S., 1997. Form finding of structural configurations possesing minimum surface area – art or science. Proc. IASS Coll. Structural Morphology: Towards the New Millennium, Nottingham.

Maurin, B., Motro, R., 1997. Density methods and minimal forms computation. Proc. IASS Coll. Structural Morphology: Towards the New Millennium, Nottingham.

Motro, R. (Ed.),1999. Tensile structures. J. Space Struct. (special issue) 14.

Oden, J.T., Sato, T., 1967. Finite strains and displacements of elastic membranes by the finite element method. Int. J. Solid Struct. 3, 87–107.

Otto, F., 1967. Tensile Structures. MIT press, Cambridge, MA.

Tabarrok, B, Qin, Z., 1992. Nonlinear analysis of tension structures. Comp. Struct. 45, 973–984.

Wakefield, D., 1979. Dynamics relaxation analysis of pretensioned networks with flexible boundaries. IASS World Congress on Shell and Spatial Structures, Madrid 1979.

Wakefield, D., 1998. Numerical modelling in tension structure design and construction. Int. Conference LSA98: Lightweight Structures in Architecture, Engineering and Construction, 1998, Sydney, pp. 1–9.